Reduced-order model for inertial locomotion of a slender swimmer

Raksha Mahalinkam, Felicity Gong, and Aditya S. Khair*
Department of Chemical Engineering, Carnegie Mellon University, Pittsburgh, Pennsylvania 15213, USA

(Received 22 January 2018; published 3 April 2018)

The inertial locomotion of an elongated model swimmer in a Newtonian fluid is quantified, wherein self-propulsion is achieved via steady tangential surface treadmilling. The swimmer has a length $2l$ and a circular cross section of longitudinal profile $a\,R(z)$, where a is the characteristic width of the cross section, $R(z)$ is a dimensionless shape function, and z is a dimensionless coordinate, normalized by l, along the centerline of the body. It is assumed that the swimmer is slender, $\epsilon = a/l \ll 1$. Hence, we utilize slender-body theory to analyze the Navier-Stokes equations that describe the flow around the swimmer. Therefrom, we compute an asymptotic approximation to the swimming speed, U, as $U/u_s = 1 - \beta[V(\mathrm{Re}) - \frac{1}{2}\int_{-1}^{1} z \ln R(z)\,dz]/\ln(1/\epsilon) + O[1/\ln^2(1/\epsilon)]$, where u_s is the characteristic speed of the surface treadmilling, Re is the Reynolds number based on the body length, and β is a dimensionless parameter that differentiates between "pusher" (propelled from the rear, $\beta < 0$) and "puller" (propelled from the front, $\beta > 0$) -type swimmers. The function $V(\mathrm{Re})$ increases monotonically with increasing Re; hence, fluid inertia causes an increase (decrease) in the swimming speed of a pusher (puller). Next, we demonstrate that the power expenditure of the swimmer increases monotonically with increasing Re. Further, the power expenditures of a puller and pusher with the same value of $|\beta|$ are equal. Therefore, pushers are superior in inertial locomotion as compared to pullers, in that they achieve a faster swimming speed for the same power expended. Finally, it is demonstrated that the flow structure predicted from our reduced-order model is consistent with that from direct numerical simulation of swimmers at intermediate Re.

DOI: 10.1103/PhysRevE.97.043102

I. INTRODUCTION

The application of reduced-order models to mathematically describe locomotion of swimming organisms was initiated by Taylor [1], who considered transverse oscillations of a two-dimensional infinite sheet as a model for flagellar propulsion at zero Reynolds number Re. Taylor's pioneering work has been generalized in many problems involving microscale propulsion, such as hydrodynamic interactions between organisms [1–4], swimming in porous media [5], transient propulsion [6], and swimming in non-Newtonian fluids [7–10]. Taylor's model was also studied at finite Re [11] and in inviscid flow (for a finite length sheet) [12,13]. In this regard, note that the fluid mechanical regimes of small and large organisms are completely different [14]. That is, the movement of microorganisms is characterized by the dominance of viscous forces over inertial forces ($\mathrm{Re} \ll 1$), whereas the reverse is true for large swimmers such as most fish. In contrast, both viscous and inertial forces play a role in the (intermediate Re) locomotion of organisms with linear dimension on the order of millimeters, including crustaceans (e.g., copepods and euphausiids), large ciliates, and small jellyfish.

The spherical squirmer, introduced by Lighthill [15] and Blake [16], is another reduced-order model for self-propulsion, where a spherical body achieves locomotion through small axisymmetric deformations of its surface. A further simplified squirmer model that swims through steady surface treadmilling (that is, steady tangential motion of its surface) has been employed to examine various facets of locomotion in Stokes ($\mathrm{Re} = 0$) flow, including enhanced diffusion of passive scalars [17,18], nutrient transport [19,20], hydrodynamic interactions of swimmers [21,22], and swimming in non-Newtonian fluids [23,24]. Furthermore, the squirmer model has recently been used to study the impact of fluid inertia on self-propulsion, using matched asymptotic expansions at small Re [25,26] and numerical computation across a wide range of Re [27]. It was found that spherical squirmers that generate thrust from their rear ("pushers") tend to swim faster than those that generate thrust from their front ("pullers") at nonzero Re.

Of course, most intermediate Re swimmers are not spherical; in fact, they tend to be elongated. The ciliate *Paramecium* roughly resembles a prolate spheroid with an approximate length and width of 100 μm and 40 μm, respectively, and has an escape swimming speed of 10 mm/s, corresponding to $\mathrm{Re} \approx 2$ [28]. Zooplankton such as copepods and krill, with length of 1 mm to 1 cm, are associated with a sustained swimming speed of around 5 cm/s and $\mathrm{Re} \approx 10$–100 [29–31]. Ngo and McHenry [32] studied the locomotion of a water boatman (*Corixidae*), which has length and width of around 5 mm and 1.5 mm, respectively. The water boatman generates thrust via paddling appendages and covers the regime $10 \lesssim \mathrm{Re} \lesssim 200$. There has been relatively little modeling work on swimming at intermediate Re, compared to the extensive literature on locomotion in Stokes flow and at large Re. Therefore, the central purpose of this article is to analyze a reduced-order model for the locomotion of a slender swimmer at nonzero Re. Naturally, such a model cannot capture in detail the locomotion of any particular organism; however, it can provide results and intuition relevant to the qualitative

*akhair@andrew.cmu.edu

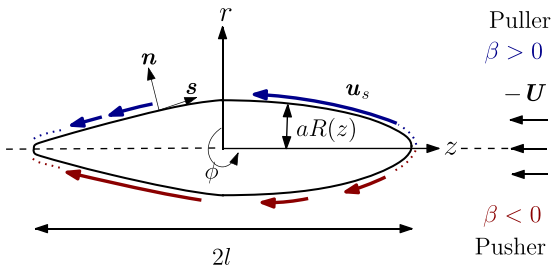

FIG. 1. Illustration of a slender squirmer-type swimmer in a comoving frame. The various symbols in this sketch are described in the main text. The curved arrows at the body surface depict the surface treadmilling stroke around a puller ($\beta > 0$) and a pusher ($\beta < 0$). For a puller (pusher), the surface velocity $\boldsymbol{u}_s$ is greatest at the front (rear) as thrust is generated from the front (rear). The dots near the ends of the body signify that $\boldsymbol{u}_s$ vanishes at the ends.

flow physics of a broad class of swimmers. As demonstrated below, the elongated form of a swimmer can be exploited to simplify the Navier-Stokes equations (NSEs) using slender-body theory, thereby allowing one to *analytically* investigate inertial locomotion. Specifically, the velocity disturbance due to the motion of an elongated body is asymptotically small in the ratio of its width to its length. This will enable us to utilize matched asymptotic expansions to predict the swimming velocity of a slender swimmer at nonzero Re. Slender-body theory is a well developed subject in Stokes flow [33–37] and in aerodynamics (Re $\gg 1$) [38,39]. Only a handful of studies have applied slender-body theory at moderate Re [40–43].

Here we consider a slender squirmer-type swimmer that has an axisymmetric body shape. A cylindrical coordinate system is adopted, where r is the radial distance and z is the axial distance, respectively, from the origin located at the center of the squirmer's body (Fig. 1). The squirmer performs a steady treadmill stroke with a surface velocity $\boldsymbol{u}_s = -u_s(1+\beta z)(\boldsymbol{s}\cdot\boldsymbol{e}_z)\boldsymbol{s}$, where u_s is the characteristic speed of the stroke. Positive values of β correspond to "pullers," while negative values of β represent "pushers" [44]. (At $\beta = 0$, the squirmer is called "neutral.") Here $\boldsymbol{e}_z$ is the unit vector in the z direction and $\boldsymbol{s}$ is the unit vector tangent to the squirmer surface. This form of surface treadmilling was used in Ref. [45] to analyze a spheroidal squirmer in Stokes flow. The Reynolds number $\mathrm{Re} = \rho u_s l/\mu$ signifies the ratio of inertial to viscous forces based on the characteristic body length l, where ρ is the fluid density and μ is the dynamic viscosity. A goal of the present study is to compute an asymptotic approximation for the swimming velocity of a squirmer, with stroke $\boldsymbol{u}_s$, as a function of Re and β. We will demonstrate that increasing Re causes an increase (decrease) in the swimming speed of a pusher (puller). This is consistent with the results obtained for a spherical squirmer [25–27]. Our assumptions of a steady surface velocity that is independent of slenderness and Reynolds number is in the spirit of providing a simple, reduced-order model of inertial locomotion. Clearly, the strokes of most biological organisms are unsteady, depend on body shape, and can vary across Re. The reasonableness of our assumptions will be verified by the demonstration that our model predicts a time-averaged, large-scale flow structure that is consistent with that from direct numerical simulation of the unsteady locomotion of intermediate Re swimmers.

In Sec. II we formulate the mathematical problem governing the locomotion of our reduced-order inertial swimmer. In Sec. III a slender-body analysis of the aforementioned problem is performed, which ultimately yields an asymptotic approximation to the swimming velocity. We discuss the results of the slender-body analysis in Sec. IV, including the swimming velocity, power expenditure, and flow structure about the swimmer. Concluding remarks and suggestions for future work are offered in Sec. V.

II. PROBLEM FORMULATION

Consider a swimmer of length $2l$ and characteristic cross-sectional width a, which achieves locomotion through steady surface treadmilling in an unbounded, incompressible Newtonian fluid. Let $\epsilon = a/l$ with $\epsilon \ll 1$; hence, the body is slender. The body has a circular cross section of radius $aR(z)$ for $-l \leqslant z \leqslant l$, where $R(z)$ is a dimensionless function that specifies the longitudinal profile of the cross section (Fig. 1). The surface velocity, or swimming stroke, $\boldsymbol{u}_s$, is independent of ϵ and Re. The squirmer swims at a velocity $\boldsymbol{U}$ in the axial direction z. In the comoving frame of the squirmer, the body is stationary, and the oncoming fluid velocity in the far field is $-\boldsymbol{U}$. Subsequent calculations are performed in this comoving frame unless stated otherwise. Only steady swimming strokes and locomotion are considered. The dimensionless NSEs and boundary conditions are

$$\mathrm{Re}\ \boldsymbol{v}\cdot\nabla\boldsymbol{v} = \nabla^2\boldsymbol{v} - \nabla p\ ,\ \nabla\cdot\boldsymbol{v} = 0, \tag{2.1}$$

$$\boldsymbol{v} \to -\boldsymbol{U} \text{ as } |\boldsymbol{x}| \to \infty, \tag{2.2}$$

$$\boldsymbol{v} = \boldsymbol{u}_s \text{ on } r = \epsilon R(z) \text{ for } -1 \leqslant z \leqslant 1, \tag{2.3}$$

where $\boldsymbol{v}$ is the velocity vector and p is the pressure. The position vector $\boldsymbol{x} = r\boldsymbol{e}_r + z\boldsymbol{e}_z$ where $\boldsymbol{e}_r$ is the unit vector in the radial direction. For steady motion of a neutrally buoyant swimmer

$$\boldsymbol{F}^H = \int \boldsymbol{\sigma}\cdot\boldsymbol{n}\, dS = 0, \tag{2.4}$$

where $\boldsymbol{F}^H$ is the hydrodynamic force, $\boldsymbol{\sigma} = -p\boldsymbol{I} + \mu[(\nabla\boldsymbol{v}) + (\nabla\boldsymbol{v})^T]$ is the stress tensor, $\boldsymbol{I}$ is the identity tensor, $(\nabla\boldsymbol{v})^T$ is the transpose of the velocity gradient $\nabla\boldsymbol{v}$, and S represents the surface of the squirmer with outward unit normal $\boldsymbol{n}$. The dimensionless equations were obtained by normalizing $\boldsymbol{v}$ and $\boldsymbol{u}_s$ by u_s, $\boldsymbol{r}$ by l, p by $\mu u_s/l$, and $\boldsymbol{\sigma}$ by $\mu u_s/l$. Henceforth, all variables and equations will be dimensionless unless otherwise stated. Since the swimming velocity is unknown *a priori*, the far-field boundary condition (2.2) cannot be applied directly. Instead, the swimming velocity is determined by applying the force-free condition (2.4).

III. SLENDER-BODY THEORY

For $\epsilon \ll 1$ the unit normal is [46]

$$\boldsymbol{n} = \boldsymbol{e}_r - \epsilon\frac{dR(z)}{dz}\boldsymbol{e}_z + O(\epsilon^2). \tag{3.1}$$

Due to axisymmetry, we write $\boldsymbol{v} = v_r\boldsymbol{e}_r + v_z\boldsymbol{e}_z$ and $\boldsymbol{u}_s = u_{sr}\boldsymbol{e}_r + u_{sz}\boldsymbol{e}_z$, where the subscripts r and z denote the radial and axial components, respectively. Since the body does not ingest or expel fluid, on S we have

$$\boldsymbol{n}\cdot\boldsymbol{v} = \boldsymbol{n}\cdot\boldsymbol{u}_s = 0. \tag{3.2}$$

Substituting (3.1) and (3.2) in the tangential velocity boundary condition $(\boldsymbol{I}-\boldsymbol{nn})\cdot\boldsymbol{v} = (\boldsymbol{I}-\boldsymbol{nn})\cdot\boldsymbol{u}_s$, we obtain from leading order matching that $v_z \sim u_{sz}$ and $v_r \sim O(\epsilon)$, where $u_{sz} = -(1+\beta z)$. Hence, the treadmilling generates a surface velocity that is purely axial, to leading order. Note that this approximation breaks down near the ends of the swimmer ($z = \pm 1$); indeed, the surface velocity field $\boldsymbol{u}_s$ vanishes at the ends. However, as discussed below, the error due to this approximation generates a contribution to the swimming speed that is subdominant to that which we calculate. As is usual in slender-body theory, the problem is partitioned into geometric inner, $r \sim O(\epsilon)$, and outer, $r \sim O(1)$, regions. In the inner region we define $\rho = r/\epsilon$ with $\rho \sim O(1)$ as $\epsilon \to 0$. From the continuity equation $\tilde{v}_r \sim \epsilon\tilde{v}_z$, i.e., the radial velocity is much smaller than the longitudinal velocity, where the tilde decoration denotes the inner region. A straightforward scaling analysis of the NSEs shows that inertial effects can be discounted in the inner region if $\epsilon^2\mathrm{Re} \ll 1$; the axial velocity then satisfies

$$\frac{1}{\rho}\frac{\partial}{\partial\rho}\left(\rho\frac{\partial\tilde{v}_z}{\partial\rho}\right) = 0, \tag{3.3}$$

subject to $\tilde{v}_z = u_{sz}$ on $\rho = R(z)$ for $-1 \leqslant z \leqslant 1$. Equation (3.3) signifies that radial diffusion of momentum governs the flow in the inner region. The solution of (3.3) is [34]

$$\tilde{v}_z = u_{sz} - \frac{F_l}{2\pi}\ln\frac{\rho}{R}, \tag{3.4}$$

where F_l is the dimensionless force per unit length exerted on the fluid by the swimmer (normalized by μu_s) acting along the z direction. In the outer region, the swimmer appears as a line segment of zero width and length 2. In terms of outer variables, the inner velocity is

$$\tilde{v}_z = u_{sz} - \frac{F_l}{2\pi}\ln\frac{1}{\epsilon} - \frac{F_l}{2\pi}\ln\frac{r}{R}. \tag{3.5}$$

Now $\ln(1/\epsilon)$ diverges as $\epsilon \to 0$, which suggests an unbounded outer flow. To prevent this absurdity, F_l must be asymptotically small in ϵ. Specifically, we require

$$-U_1 \sim u_{sz} - \frac{F_l}{2\pi}\ln\frac{1}{\epsilon}, \tag{3.6}$$

where $U_1\boldsymbol{e}_z$ is the leading order contribution to the swimming velocity. The force per unit length is then

$$F_l = \frac{f_1}{\ln\frac{1}{\epsilon}} \tag{3.7}$$

to leading order, where $f_1 = 2\pi(U_1 + u_{sz})$. The constraint (2.4) implies $\int_{-1}^{1} f_1\,dz = 0$. Therefore,

$$U_1 = -\frac{1}{2}\int_{-1}^{1} u_{sz}\,dz. \tag{3.8}$$

Using $u_{sz} = -(1+\beta z)$, we find that $U_1 = 1$, regardless of the value of β. Thus, to leading order, the swimming velocity of a slender squirmer is independent of whether it is a pusher or puller. Theers *et al.* [45] derived an expression for the swimming velocity of a prolate spheroidal squirmer, of arbitrary aspect ratio, with surface velocity $\boldsymbol{u}_s$ in Stokes flow [see Eq. (29) in their paper]. Their result reduces to ours (i.e., $U_1 \sim 1$) in the limit of a slender spheroid. Additionally, our analysis shows to leading order in ϵ that (1) the independence of the swimming velocity on β holds at nonzero Re and (2) the swimming velocity is independent of the longitudinal radius profile $R(z)$. Leshansky *et al.* [47] also considered a prolate spheroidal swimmer at $\mathrm{Re} = 0$, propelled by surface treadmilling for the case $\beta = 0$. They too found that $U_1 \sim 1$ for a slender swimmer, with an algebraically small error of $\epsilon^2\ln(1/\epsilon)$ arising from the flow near the ends of the body. They commented that the physical meaning of this result is that the swimmer is propelled with the velocity of surface treadmilling, such that surface velocity in laboratory frame is nearly zero over the majority of the body. Such a situation leads to, in their words, a nearly "frictionless microswimmer" with a power expenditure that is algebraically small in ϵ. Finally, note that the swimming velocity of a spherical squirmer is also independent of β in Stokes flow [15,26,48].

The above arguments suggest expansions of the force per unit length and velocity field in powers of $1/\ln(1/\epsilon)$. Since the inner region is viscously dominated provided $\epsilon^2\mathrm{Re} \ll 1$, the solution (3.4) remains valid with now a "weak" expansion of F_l in $1/\ln(1/\epsilon)$. In contrast, in the outer region we expand

$$\boldsymbol{v} \sim -\boldsymbol{e}_z + \frac{1}{\ln\frac{1}{\epsilon}}\boldsymbol{v}_2 + \cdots, \quad p \sim \frac{1}{\ln\frac{1}{\epsilon}}p_2 + \cdots, \tag{3.9}$$

where $\boldsymbol{v}_2$ and p_2 are the $O[1/\ln(1/\epsilon)]$ contributions to the velocity and pressure fields, respectively. By substituting the expansions (3.9) into the NSEs (2.1), we find that the $O[1/\ln(1/\epsilon)]$ flow in the outer region is governed by the Oseen equations,

$$-\mathrm{Re}\frac{\partial\boldsymbol{v}_2}{\partial z} = \nabla^2\boldsymbol{v}_2 - \nabla p_2, \quad \nabla\cdot\boldsymbol{v}_2 = 0, \tag{3.10}$$

subject to

$$\boldsymbol{v}_2 \to -U_2\boldsymbol{e}_z \text{ as } |\boldsymbol{x}| \to \infty, \tag{3.11}$$

where U_2 is the $O[1/\ln(1/\epsilon)]$ contribution to the swimming speed. The solution to (3.10) will be matched to the inner solution. The solution of the Oseen equations for a point force $F\delta(\boldsymbol{x})\boldsymbol{e}_z$ at the origin, where $\delta(\boldsymbol{x})$ is the Dirac delta function and F is the strength of the point force, yields the "Oseenlet" velocity field [49]

$$\frac{F\boldsymbol{e}_z}{4\pi|\boldsymbol{x}|}\mathrm{e}^{-\frac{\mathrm{Re}}{2}[z-|\boldsymbol{x}|]} + \frac{F}{4\pi\mathrm{Re}}\nabla\left(\frac{\mathrm{e}^{-\frac{\mathrm{Re}}{2}[z-|\boldsymbol{x}|]}-1}{|\boldsymbol{x}|}\right). \tag{3.12}$$

Since the Oseen equations are linear, the outer velocity field is constructed as a distribution of Oseenlets along the centerline

of the body,

$$\boldsymbol{v}_2(\boldsymbol{x}) = -U_2\boldsymbol{e}_z + \frac{\boldsymbol{e}_z}{4\pi}\int_{-1}^{1} g(\zeta)\frac{e^{-\frac{\mathrm{Re}}{2}\{(z-\zeta)+[r^2+(z-\zeta)^2]^{1/2}\}}}{[r^2+(z-\zeta)^2]^{1/2}}\,d\zeta + \frac{1}{4\pi\,\mathrm{Re}}\nabla\int_{-1}^{1} g(\zeta)\frac{[e^{-\frac{\mathrm{Re}}{2}\{(z-\zeta)+[r^2+(z-\zeta)^2]^{1/2}\}}-1]}{[r^2+(z-\zeta)^2]^{1/2}}\,d\zeta, \tag{3.13}$$

where $g(z)$ is the source density of Oseenlets per unit length. The axial component of $\boldsymbol{v}_2$ is

$$v_{2z} = -U_2 + \frac{1}{4\pi}I_1 + \frac{1}{4\pi\,\mathrm{Re}}\frac{\partial I_2}{\partial z}, \tag{3.14}$$

where I_1 and I_2 denote the first and second integrals, respectively, appearing in (3.13).

We seek the limit of v_{2z} as $r \to 0$ for matching to the inner solution (3.4). This requires finding the limiting forms of the integrals I_1 and I_2 as $r \to 0$. Now I_1 is singular as $r \to 0$; its asymptotic behavior can be extracted following the approach of Schnitzer [50]: see Eqs. (3.9) and (3.10) and the accompanying discussion in that paper. The integral I_2 is regular as $r \to 0$; its leading order asymptotic behavior as $r \to 0$ is found by setting $r = 0$ in the integrand. Therefore, we obtain

$$I_1 = 2g(z)\ln\left[\frac{2(1-z^2)^{1/2}}{r}\right] + J_1 + o(1) \tag{3.15}$$

and

$$I_2 = J_2 + o(1), \tag{3.16}$$

where

$$J_1 = \int_{-1}^{1}\frac{g(\zeta)e^{-\frac{\mathrm{Re}}{2}[(z-\zeta)+|z-\zeta|]} - g(z)}{|z-\zeta|}\,d\zeta\,,$$
$$J_2 = \int_{-1}^{1} g(\zeta)\left[\frac{e^{-\frac{\mathrm{Re}}{2}[(z-\zeta)+|z-\zeta|]}-1}{|z-\zeta|}\right]d\zeta. \tag{3.17}$$

The inner limit of the outer velocity field is hence

$$v_{2z} \sim -U_2 - \frac{1}{4\pi}g(z)2\ln r + \frac{1}{4\pi}\left\{g(z)2\ln[2(1-z^2)^{1/2}] + J_1 + \frac{1}{\mathrm{Re}}\frac{\partial J_2}{\partial z}\right\} + o(1). \tag{3.18}$$

Writing the inner expansion in terms of outer variables gives

$$\tilde{v}_z \sim u_{sz} - \frac{1}{2\pi}\left[\frac{f_1}{\ln\frac{1}{\epsilon}} + \frac{f_2}{\left(\ln\frac{1}{\epsilon}\right)^2} + \cdots\right]\left[\ln\frac{1}{\epsilon} + \ln\frac{r}{R}\right], \tag{3.19}$$

where f_2 is the $O(1/\ln^2(1/\epsilon))$ contribution to the force per unit length. Matching terms of $O(1/\ln(1/\epsilon))$ from the inner and outer expansions yields

$$g(z) = -2\pi\beta z \tag{3.20}$$

and

$$f_2 = 2\pi\left[U_2 + \beta z\ln\frac{2(1-z^2)^{1/2}}{R}\right] - \frac{1}{2}\left[J_1 + \frac{1}{\mathrm{Re}}\frac{\partial J_2}{\partial z}\right]. \tag{3.21}$$

The source density $g(z)$ vanishes for a neutral squirmer, in which case the trivial solution $\boldsymbol{v}_2(\boldsymbol{x}) = 0$ holds. Hence, $U_2 = 0$; there is no $O(1/\ln(1/\epsilon))$ contribution to the swimming velocity. Moreover, for $\beta = 0$ all higher-order terms in the weak expansion of the swimming velocity vanish, which implies that the correction to the leading order swimming velocity, $U = 1$, is algebraically small in ϵ. This is in agreement with the calculations of Leshansky *et al.* [47] for a spheroidal swimmer in Stokes flow. In fact, the present swimmer problem for $\beta = 0$ is equivalent to irrotational flow past a slender obstacle, for which the disturbance to the free stream velocity is algebraically small in the slenderness [46]. The swimmer does cause an $O[1/\ln(1/\epsilon)]$ flow disturbance at nonzero β; hence, one expects a correction to the swimming speed at this order, generally. Physically, for $\beta \neq 0$ the swimmer acts as a source of vorticity, which diffuses through the inner region and is then advected past the swimmer in the outer region (at nonzero Re). There is no stretching of vorticity in the outer region as the leading order flow therein is a uniform stream. More specifically, since $g(z)$ is a linear function of z whose integral along the body length is zero, the force-free swimmer represents a quadrupole source of vorticity. In Stokes flow the evolution of vorticity in the fluid is solely via diffusion; hence, the fore-aft (anti)symmetry of the quadrupole (for a swimmer with a fore-aft symmetric longitudinal radius profile) is retained and dictates that there is no net effect on the swimming speed. That is, we expect $U_2 = 0$ at $\mathrm{Re} = 0$ for all fore-aft symmetric pushers or pullers. At nonzero Re the antisymmetric vorticity distribution in the fluid is broken by inertial forces; hence, there will be a nonzero contribution to the swimming speed at finite Reynolds number. Moreover, since the source distribution is reversed in sign, but unaltered in magnitude, under the transformation $\beta \to -\beta$, we expect pushers and pullers with the same value $|\beta|$ to have an inertial contribution to U_2 that is equal in magnitude but opposite in sign. These predictions will be verified in the calculations below.

Using (3.20) we evaluate the integrals J_1 and J_2 (3.17) as

$$\frac{J_1(z)}{2\pi\beta} = z\{\ln[\mathrm{Re}(z+1)] + \gamma + E_1[\mathrm{Re}(z+1)]\} + z - 1 + \frac{1}{\mathrm{Re}}(1 - e^{-\mathrm{Re}(z+1)}) \tag{3.22}$$

and

$$\frac{J_2(z)}{2\pi\beta} = \frac{J_1(z)}{2\pi\beta} - 2z, \tag{3.23}$$

where $\gamma = 0.577\ldots$ is the Euler-Mascheroni constant, and $E_1(x) = \int_x^\infty t^{-1}e^{-t}\,dt$ is the exponential integral. As Re increases the variation of J_1 and J_2 with z becomes increasingly nonlinear, signifying the increasing impact of inertia on the flow (Fig. 2).

Since the swimmer is force-free, $\int_{-1}^{1} f_2\,dz = 0$. Hence, using (3.21) with (3.22) and (3.23) yields the $O[1/\ln(1/\epsilon)]$ contribution to the swimming speed as

$$U_2 = \beta\left[\frac{1}{2}\int_{-1}^{1} z\ln R(z)\,dz - V(\mathrm{Re})\right], \tag{3.24}$$

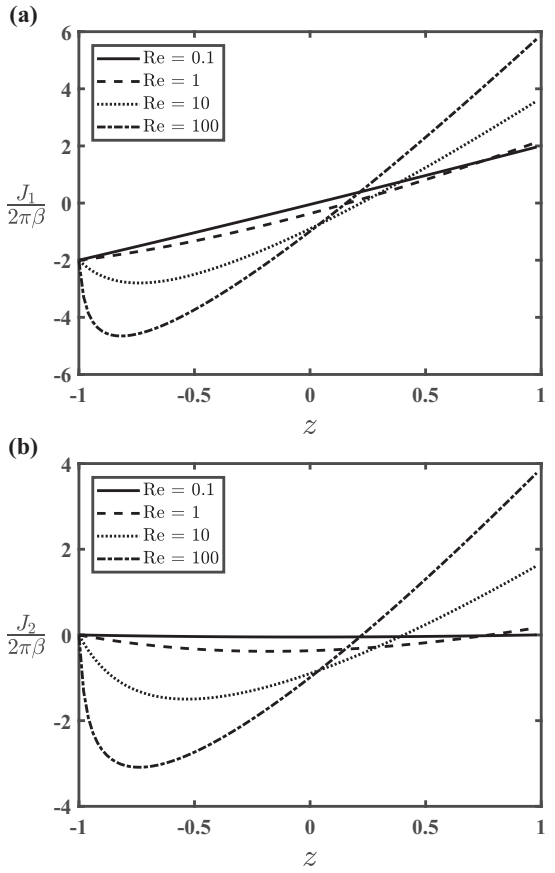

FIG. 2. Plots of J_1 (a) and J_2 (b) versus z for various Re. The functions $J_1(z)$ and $J_2(z)$ are defined in (3.22) and (3.23), respectively, and appear in the $O[1/\ln^2(1/\epsilon)]$ contribution to the force per unit length f_2 (3.21).

where

$$V(\mathrm{Re}) = \frac{1}{8\mathrm{Re}^2}(\mathrm{e}^{-2\mathrm{Re}} + 2\mathrm{Re}^2 + 2\mathrm{Re} - 1) - \frac{1}{4\mathrm{Re}}[\ln(2\mathrm{Re}) + \gamma + E_1(2\mathrm{Re})] \quad (3.25)$$

depends on Re but is independent of β and the profile $R(z)$. The total swimming speed is

$$U = 1 + \frac{U_2}{\ln\frac{1}{\epsilon}} + O\left[\frac{1}{(\ln\frac{1}{\epsilon})^2}\right]. \quad (3.26)$$

From (3.24), the first term of U_2 is independent of Re and vanishes for a swimmer with a fore-aft symmetric radius profile. The influence of inertia on the swimming speed is therefore encapsulated in the function $V(\mathrm{Re})$ (Fig. 3). For small Re

$$V(\mathrm{Re}) = \frac{\mathrm{Re}}{12} + O(\mathrm{Re}^2), \quad (3.27)$$

and at large Re

$$V(\mathrm{Re}) = \frac{1}{4} + O(\mathrm{Re}^{-1}\ln\mathrm{Re}). \quad (3.28)$$

It is interesting that $V(\mathrm{Re})$ remains bounded as $\mathrm{Re}\to\infty$. This is in contrast to the equivalent slender-body analysis of

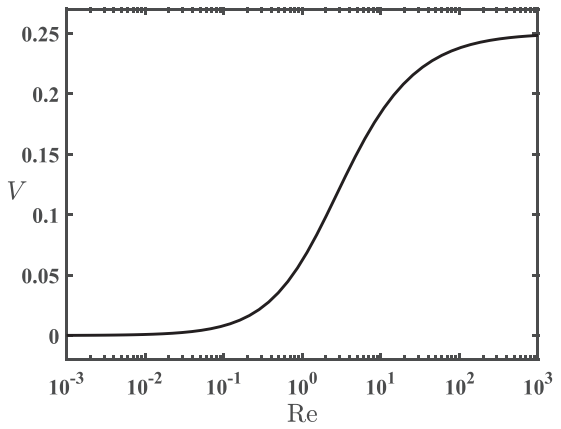

FIG. 3. Plot of V versus Re. The function $V(\mathrm{Re})$ is defined in (3.25) and represents the inertial contribution to the $O[1/\ln(1/\epsilon)]$ swimming speed U_2.

the drag on particle towed by an external force, where the second approximation to the drag grows as $\ln(\mathrm{Re})$ at $\mathrm{Re}\gg 1$ [40]. This logarithmic divergence implies that the asymptotic expansion for the drag loses uniformity at $\epsilon\mathrm{Re} = O(1)$, i.e., when the Reynolds number based on the cross-sectional radius is order one. No such loss of uniformity occurs in the swimmer problem; here the looser constraint $\epsilon^2\mathrm{Re}\ll 1$ is required so that viscous forces dominate inertial forces in the inner region. The difference is that the towed particle exerts a net force on the fluid, unlike the swimmer, which is force-free.

IV. RESULTS

A. Swimming velocity

A number of the predictions made above are now verifiable. First, $U_2 = 0$ for a neutral squirmer. Second, the values of $|U_2|$ for a pusher and puller with equal values of $|\beta|$ are identical. Third, for a fore-aft symmetric body, $U_2 = 0$ at $\mathrm{Re} = 0$ and monotonically increases (in magnitude) with increasing Re for a given β, due to the increasing effectiveness of inertial forces in sweeping vorticity past the swimmer. At fixed Re, the magnitude of U_2 increases with increasing magnitude of β, as the swimmer acts as a stronger source of vorticity. Finally, U_2 increases (decreases) monotonically for pushers (pullers) with increasing Re. This can be explained by analyzing the $O[1/\ln^2(1/\epsilon)]$ inertial thrust per unit length exerted *by* the fluid *on* the swimmer, T_I, defined as

$$T_I = -\left[f_2 - 2\pi\left\{U_2 + \beta z\ln\left[\frac{2(1-z^2)^{1/2}}{R(z)}\right] - \frac{3\beta z}{2}\right\}\right]. \quad (4.1)$$

Hence, using (3.21), (3.22), and (3.23) with (4.1) we find that

$$\frac{T_I}{2\pi\beta} = \frac{1}{2\mathrm{Re}}\frac{z}{z+1}(1-\mathrm{e}^{-\mathrm{Re}(z+1)}) - \left(z+\frac{1}{2}\right) + \frac{1}{2}\left(z+\frac{1}{\mathrm{Re}}\right)\{\ln[\mathrm{Re}(z+1)] + \gamma + E_1[\mathrm{Re}(z+1)]\}. \quad (4.2)$$

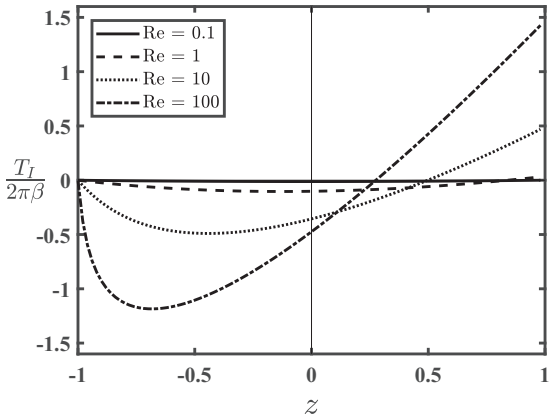

FIG. 4. Distribution of inertial thrust per unit length T_I at various Re. The thin vertical line at $z = 0$ is to help the reader visualize the increasing left-right asymmetry in T_I with increasing Re.

Note that $T_I/2\pi\beta = (z^2 - 1)\mathrm{Re}/8 + O(\mathrm{Re}^2)$ at small Re; thus it is a purely inertial quantity. The function T_I is plotted in Fig. 4. It is readily shown that $\int_{-1}^{1} T_I\, dz$ is positive for a pusher at nonzero Re, which is consistent with U_2 being positive. That is, the fluid exerts an inertial thrust on a pusher in the positive z direction, which must be balanced by additional drag in the negative z direction so that the swimmer remains force-free. This additional drag is achieved by an increase in the swimming speed of a pusher. The reverse is true for a puller. Therefore, fluid inertia cases an increase (decrease) in the swimming speed of a pusher (puller). The origin of the inertial thrust lies in the vorticity field around the swimmer. Recall that at $\mathrm{Re} = 0$ the vorticity bears a fore-aft antisymmetric quadrupole distribution, decaying as $1/|\boldsymbol{x}|^3$ at large distances from the swimmer. (Here we ignore higher order multipoles associated with a fore-aft asymmetric body shape, which do not generate a contribution to the inertial thrust at the present level of approximation.) More precisely, the vorticity field is made up of two counter-rotating sets of vortex rings, as depicted in Fig. 5(a) for a pusher. The antisymmetry of the vorticity dictates that the pusher contribution to the stroke, namely, $u_{sz} + 1 = -\beta z$, does not affect the swimming velocity, which is thus independent of β. The inertial thrust is a consequence of the loss of this antisymmetry at nonzero Re, as vorticity is advected to the rear of the swimmer [Fig. 5(b)]. For a pusher, the sets of counter-rotating vortex rings generate a flow toward the rear body surface that has a component in the positive z direction. It is this flow that drives the positive inertial thrust T_I for a pusher, causing an increase in its swimming speed with increasing Re. Conversely, for a puller, the flow generated by the counter-rotating vortices has a component in the negative z direction, which leads to a decrease in the swimming speed.

B. Power expenditure

The dimensionless power, P, expended by the swimmer (normalized by $\mu u_s^2 l$) is [47]

$$P = -\int \boldsymbol{n}\cdot\boldsymbol{\sigma}\cdot\boldsymbol{u}_s\, dS. \tag{4.3}$$

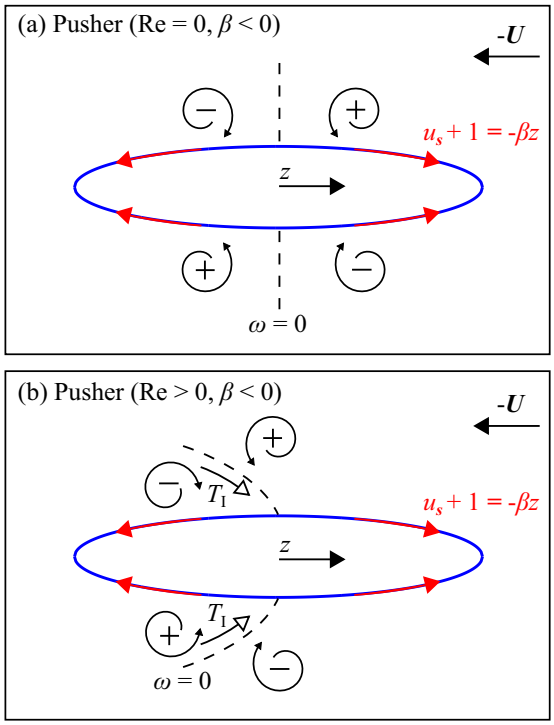

FIG. 5. Mechanism of inertial thrust generation for a pusher. (a) At $\mathrm{Re} = 0$ the pusher contribution to the stroke, $u_{sz} + 1 = -\beta z$ (shown by curved arrows on the body surface), results in a fore-aft antisymmetric vorticity distribution, as depicted by the oppositely signed, counter-rotating vortices. In particular, the magnitude of the vorticity is zero at the midpoint of the body, as indicated by the dashed vertical line where $\omega = 0$. (b) At $\mathrm{Re} > 0$ vorticity is advected past the swimmer by inertial forces, such that the fore-aft antisymmetry is lost. Hence, as explained in the main text, an inertial thrust T_I is generated that leads to an increase in the swimming speed. An equivalent argument can readily be made to explain the decrease in the swimming speed of a puller with increasing Re.

In the slender-body approximation we find

$$P = -\beta \int_{-1}^{1} z F_l\, dz. \tag{4.4}$$

Substituting the weak expansion for F_l we obtain

$$P = \frac{p_1}{\ln\frac{1}{\epsilon}} + \frac{p_2}{(\ln\frac{1}{\epsilon})^2} + O\left[\frac{1}{(\ln\frac{1}{\epsilon})^3}\right], \tag{4.5}$$

where $p_1 = 4\pi\beta^2/3$ and $p_2 = -\beta\int_{-1}^{1} z f_2\, dz$. Using (3.21) yields

$$\frac{p_2}{2\pi\beta^2} = W(\mathrm{Re}) + \int_{-1}^{1}\left\{\frac{1}{2} - z^2\ln\left[\frac{2(1-z^2)^{1/2}}{R(z)}\right]\right\} dz, \tag{4.6}$$

where

$$W(\mathrm{Re}) = \left(\frac{1}{3} + \frac{1}{2\mathrm{Re}}\right)\left[\ln(2\mathrm{Re}) + \gamma + E_1(2\mathrm{Re})\right] + \frac{3 - 40\mathrm{Re}^3}{36\mathrm{Re}^3} - \left(\frac{1 + 2\mathrm{Re} + 2\mathrm{Re}^2}{12\mathrm{Re}^3}\right)\mathrm{e}^{-2\mathrm{Re}} \tag{4.7}$$

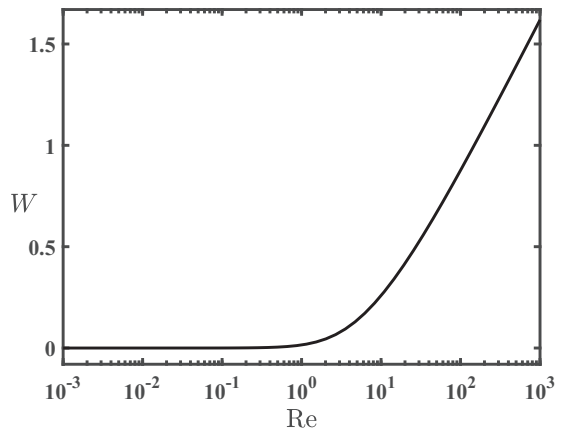

FIG. 6. Plot of W versus Re. The function $W(\mathrm{Re})$ is defined in (4.7) and represents the inertial contribution to the $O[1/\ln^2(1/\epsilon)]$ power expenditure p_2.

encapsulates the influence of inertial forces on the power expenditure All terms in the weak expansion of P vanish for a neutral swimmer; here the power expended is algebraically small in ϵ, due to small dissipation at the ends of the swimmer, which are neglected in our analysis. This is consistent with the finding of Leshansky *et al.* [47] that a slender $\beta = 0$ swimmer is almost "frictionless." At nonzero β, the addition of a puller or pusher contribution to the stroke leads to a power expenditure that is logarithmically small in ϵ. Evidently, p_1 and p_2 are equal for a pusher and puller with the same value of $|\beta|$. At $O[1/\ln(1/\epsilon)]$ the power expenditure is independent of Re, but this is not so at $O[1/\ln^2(1/\epsilon)]$, where W is a monotonically increasing function of Re (Fig. 6). Therefore, the power expended by the swimmer increases with increasing Re. In fact, at small Re

$$W(\mathrm{Re}) = \frac{\mathrm{Re}^2}{45} + O(\mathrm{Re}^3), \tag{4.8}$$

and at large Re

$$W(\mathrm{Re}) = \frac{1}{3}\left[\ln(2\mathrm{Re}) + \gamma - \frac{10}{3}\right] + O(\mathrm{Re}^{-1}\ln\mathrm{Re}). \tag{4.9}$$

The logarithmic divergence of W at large Re implies that the expansion for P (4.5) loses uniformity at $\mathrm{Re} = O(1/\epsilon)$. It is interesting that, in contrast, the expansion for the swimming speed U (3.26) does not lose uniformity at $\mathrm{Re} = O(1/\epsilon)$, for reasons explained above.

C. Far-field flow

It is instructive to examine the flow at large distances from the swimmer, $\mathrm{Re}|\boldsymbol{x}| \gg 1$. In the laboratory frame the flow attenuates at large distances, and the velocity decay is found from (3.13). In the majority, or "bulk," of the far-field the exponential terms in the integrands of I_1 and I_2 are negligibly small. Therefore, I_1 can be neglected altogether, and expanding the remaining portion of the integrand of I_2 for $\mathrm{Re}|\boldsymbol{x}| \gg 1$ shows that the bulk flow degenerates to a potential dipole

$$\boldsymbol{v}_{\mathrm{bulk}} \sim \frac{\beta}{3\mathrm{Re}\ln(1/\epsilon)}\boldsymbol{e}_z\cdot\left(\frac{\boldsymbol{I}}{|\boldsymbol{x}|^3} - \frac{3\boldsymbol{x}\boldsymbol{x}}{|\boldsymbol{x}|^5}\right), \tag{4.10}$$

which results in an irrotational velocity field decaying as $1/|\boldsymbol{x}|^3$. Therefore, for $\mathrm{Re}|\boldsymbol{x}| \gg 1$ the vorticity generated by the swimmer is confined to a narrow wake at the aft symmetry axis, where $1 + \cos\theta \sim O(1/\mathrm{Re}|\boldsymbol{x}|)$. Here θ is the polar angle measured from the z axis. The flow in the wake arises solely from the second term in (3.13), since the third term is a gradient field and hence produces an irrotational flow. [The first term in (3.13) is a uniform flow and hence makes no contribution to the far-field flow in the laboratory frame.] Therefore, expanding the second term for large $\mathrm{Re}|\boldsymbol{x}|$ with $\mathrm{Re}|\boldsymbol{x}|(1+\cos\theta) = O(1)$ yields the wake velocity field

$$\boldsymbol{v}_{\mathrm{wake}} \sim \frac{\beta\boldsymbol{e}_z}{3\ln(1/\epsilon)}\frac{1}{z^2}\left(1 + \frac{\mathrm{Re}r^2}{4z}\right)\mathrm{e}^{\mathrm{Re}r^2/4z}, \tag{4.11}$$

in which $|\boldsymbol{x}| \approx -z$ and $z < 0$ near the aft symmetry axis. The velocity disturbance in the wake is purely axial and decays as $1/|\boldsymbol{x}|^2$, as opposed to the faster $1/|\boldsymbol{x}|^3$ decay outside the wake. The velocity in the wake changes direction at $r = 2\sqrt{-z/\mathrm{Re}}$: for a pusher the flow is opposite the direction of locomotion for $r < 2\sqrt{-z/\mathrm{Re}}$; the opposite is true for a puller. The mass deficit in the wake is zero, which is consistent with the flow in the bulk being solenoidal. Likewise, the wake does not contain a momentum deficit, since the swimmer is force-free. Recall that the velocity field in the wake behind a particle subject to an external force decays as $1/|\boldsymbol{x}|$ and contains a momentum deficit that is proportional to the drag on the particle. The vorticity in the wake $\boldsymbol{\omega}_{\mathrm{wake}} = \omega_{\mathrm{wake}}\boldsymbol{e}_\phi$, where $\boldsymbol{e}_\phi$ is the azimuthal unit vector about the symmetry axis. From (4.11),

$$\omega_{\mathrm{wake}} \sim -\frac{2\beta}{3\ln(1/\epsilon)}\frac{\mathrm{Re}\,r}{4z^3}\left(2 + \frac{\mathrm{Re}r^2}{4z}\right)\mathrm{e}^{\mathrm{Re}r^2/4z}. \tag{4.12}$$

The vorticity decays as $1/|\boldsymbol{x}|^3$ and vanishes at $r = 0, \sqrt{-8z/\mathrm{Re}}$.

The far-field flow predicted from our reduced-order model is consistent with direct numerical simulations (DNSs) of swimmers at moderate Reynolds numbers. Yeo *et al.* [51] conducted DNSs of the swimming of a carangiform fish for Re between 100 to 5000. Outside the wake and away from the immediate vicinity of the fish, the flow strongly resembles a potential dipole (see Figs. 16 and 20 in their paper), as we predict (4.10). The unsteady flow in the wake adopts the form of a reverse von Kármán vortex street, in which the sign of the vortices are reversed from the vortex street behind a (nonswimming) bluff body [52]. Similar DNSs of Maertens *et al.* [53] demonstrate that the time-averaged flow in the wake of an undulating fish gives an axial velocity profile that moves away from the swimmer near the centerline of the body (i.e., an outward jet), but then reverses sign to ultimately yield a wake that is momentumless. This averaged flow is consistent with what we predict for a pusher (4.11), where the velocity has a zero crossing in the wake and is directed away from the swimmer near the centerline. Indeed, a carangiform fish generates thrust by undulations of its caudal (tail) region, with relatively little movement of other parts of its body, which is consistent with our model in which the surface velocity is largest at the rear of a pusher. Maertens *et al.* [53] also demonstrate that the time-averaged vorticity field in the wake is characterized by a quartet of shear layers of alternating sign. This is again consistent with the vorticity

structure that we predict (4.12), which has two zero crossings in the wake, demarcating regions of oppositely signed vortices. The occurrence of four shear layers is a manifestation of that fact that the swimmer acts a quadrupole source of vorticity, as discussed above.

V. CONCLUSION

We have utilized slender-body theory to analyze the locomotion of a model elongated swimmer at nonzero Reynolds number. The swimmer achieves self-propulsion by steady surface treadmilling. We find that a pusher is superior to a puller in inertial locomotion, since both expend the same power (for equal values of $|\beta|$), while the pusher (puller) swims faster (slower) with increasing Re. This finding may be of relevance in the design of gaits for artificial swimmers in inertial flow regimes. On that note, it would be interesting to consider surface velocities that depend on ϵ and Re, to mimic the differences in gaits exhibited by organisms across Re. A more important extension would be to model unsteady treadmilling of slender swimmers at finite Re, which is of clear relevance since nearly all biological swimmers self-propel via time-dependent gaits. Here we note that recent work has considered a slender-body theory for the unsteady Stokes equations, with application toward locomotion of microorganisms [54]. A sensible first step for inertial locomotion would be to construct a slender-body theory for the unsteady Oseen equations. However, while analysis of unsteady gaits is of practical interest, we reemphasize that our simple model does capture the time-averaged flow structure of intermediate Re swimmers.

ACKNOWLEDGMENTS

A.S.K. acknowledges support from the Camille Dreyfus Teacher-Scholar Award program. F.G. acknowledges support from the Summer Undergraduate Research Fellowship program at Carnegie Mellon University.

[1] G. Taylor, Proc. R. Soc. Lond. **209**, 447 (1951).
[2] G. J. Elfring and E. Lauga, Phys. Rev. Lett. **103**, 088101 (2009).
[3] G. J. Elfring, O. S. Pak, and E. Lauga, J. Fluid Mech. **646**, 505 (2010).
[4] V. Gyrya, I. S. Aranson, L. V. Berlyand, and D. Karpeev, Bull. Math. Biol. **72**, 148 (2010).
[5] A. M. Leshansky, Phys. Rev. E **80**, 051911 (2009).
[6] O. S. Pak and E. Lauga, Proc. R. Soc. Lond. A **466**, 107 (2010).
[7] E. Lauga, Phys. Fluids **19**, 083104 (2007).
[8] H. C. Fu, C. W. Wolgemuth, and T. R. Powers, Phys. Fluids **21**, 033102 (2009).
[9] H. C. Fu, V. B. Shenoy, and T. R. Powers, EPL (Europhys. Lett.) **91**, 24002 (2010).
[10] J. Teran, L. Fauci, and M. Shelley, Phys. Rev. Lett. **104**, 038101 (2010).
[11] S. Childress, in *Proc. ASME 2008 Dynamic Systems and Control Conf., Ann Arbor, Michigan, USA* (2008), pp. 20–22.
[12] T. Y.-T. Wu, J. Fluid Mech. **10**, 321 (1961).
[13] T. Y.-T. Wu, J. Fluid Mech. **46**, 337 (1971).
[14] S. Childress, *Mechanics of Swimming and Flying*, Vol. 2 (Cambridge University Press, Cambridge, 1981).
[15] M. Lighthill, Commun. Pure Appl. Maths **5**, 109 (1952).
[16] J. Blake, J. Fluid Mech. **46**, 199 (1971).
[17] J.-L. Thiffeault and S. Childress, Phys. Lett. A **374**, 3487 (2010).
[18] Z. Lin, J.-L. Thiffeault, and S. Childress, J. Fluid Mech. **669**, 167 (2011).
[19] V. Magar, T. Goto, and T. Pedley, Q. J. Mech. Appl. Maths **56**, 65 (2003).
[20] V. Magar and T. Pedley, J. Fluid Mech. **539**, 93 (2005).
[21] T. Ishikawa, M. Simmonds, and T. Pedley, J. Fluid Mech. **568**, 119 (2006).
[22] K. Drescher, K. C. Leptos, I. Tuval, T. Ishikawa, T. J. Pedley, and R. E. Goldstein, Phys. Rev. Lett. **102**, 168101 (2009).
[23] L. Zhu, M. Do-Quang, E. Lauga, and L. Brandt, Phys. Rev. E **83**, 011901 (2011).
[24] L. Zhu, E. Lauga, and L. Brandt, Phys. Fluids **24**, 051902 (2012).
[25] S. Wang and A. Ardekani, Phys. Fluids **24**, 101902 (2012).
[26] A. S. Khair and N. G. Chisholm, Phys. Fluids **26**, 011902 (2014).
[27] N. G. Chisholm, D. Legendre, E. Lauga, and A. S. Khair, J. Fluid Mech. **796**, 233 (2016).
[28] A. Hamel, C. Fisch, L. Combettes, P. Dupuis-Williams, and C. N. Baroud, Proc. Natl Acad. Sci. USA **108**, 7290 (2011).
[29] W. M. Hamner, J. Crustac. Biol. **4**, 67 (1984).
[30] M. E. Huntley and M. Zhou, Mar. Ecol. **273**, 65 (2004).
[31] E. Kunze, J. Mar. Res. **69**, 591 (2011).
[32] V. Ngo and M. J. McHenry, J. Exp. Biol. **217**, 2740 (2014).
[33] E. Tuck, J. Fluid Mech. **18**, 619 (1964).
[34] G. Batchelor, J. Fluid Mech. **44**, 419 (1970).
[35] R. Cox, J. Fluid Mech. **44**, 791 (1970).
[36] J. Tillett, J. Fluid Mech. **44**, 401 (1970).
[37] R. E. Johnson, J. Fluid Mech. **99**, 411 (1980).
[38] M. D. Van Dyke, *Perturbation Methods in Fluid Mechanics* (Parabolic Press, Stanford, 1975).
[39] D. Degani and Y. Levy, J. AIAA **30**, 2267 (1992).
[40] R. Khayat and R. Cox, J. Fluid Mech. **209**, 435 (1989).
[41] G. Subramanian and D. L. Koch, J. Fluid Mech. **535**, 383 (2005).
[42] M. Shin, D. L. Koch, and G. Subramanian, J. Phys. Fluids **18**, 063301 (2006).
[43] M. Shin, D. L. Koch, and G. Subramanian, J. Phys. Fluids **21**, 123304 (2009).
[44] T. Ishikawa and T. J. Pedley, J. Fluid Mech. **588**, 399 (2007).
[45] M. Theers, E. Westphal, G. Gompper, and R. G. Winkler, J. Soft Matter **12**, 7372 (2016).
[46] E. J. Hinch, *Perturbation Methods* (Cambridge University Press, Cambridge, 1991).
[47] A. M. Leshansky, O. Kenneth, O. Gat, and J. E. Avron, New J. Phys. **9**, 145 (2007).
[48] G. Li, A. Ostace, and A. M. Ardekani, Phys. Rev. E **94**, 053104 (2016).
[49] D. Homentcovschi, SIAM J. Appl. Maths **40**, 99 (1981).
[50] O. Schnitzer, J. Fluid Mech. **768**, R5 (2015).
[51] K. S. Yeo and S. J. A. Chu, Comput. Fluids **39**, 403 (2011).
[52] C. Eloy, J. Fluids Struct. **30**, 205 (2012).
[53] A. P. Maertens, A. Gao, and M. S. Triantafyllou, J. Fluid Mech. **813**, 301 (2017).
[54] E. Barta, J. Fluid Mech. **688**, 66 (2011).